Science Signaling AAAS

www.sciencesignaling.org/cgi/content/full/4/183/ra49/DC1

Supplementary Materials for

A Cell-Based High-Content Screening Assay Reveals Activators and Inhibitors of Cancer Cell Invasion

Manuela Quintavalle, Leonardo Elia, Jeffrey H. Price, Susanne Heynen-Genel, Sara A. Courtneidge*

*To whom correspondence should be addressed. E-mail: courtneidge@sanfordburnham.org

Published 26 July 2011, *Sci. Signal.* **4**, ra49 (2011)
DOI: 10.1126/scisignal.2002032

The PDF file includes:

Fig. S1. Statistics of positive (inhibited) and negative (uninhibited) control cell populations for rosette detection.
Fig. S2. Detailed analysis of the HCS results.
Fig. S3. Effect of purvalanol A on the cell cycle.
Fig. S4. p35 abundance and localization in Src-3T3 cells.
Fig. S5. Effect of Cdk5 knockdown on formation and function of invadopodia.
Fig. S6. Effect of purvalanol A on Cdk5 activity.
Fig. S7. Phosphorylation of caldesmon by Cdk5 regulates formation of invadopodia.
Fig. S8. Knockdown of caldesmon rescues formation of invadopodia in cells deficient in Cdk5.
Table S1. Statistics for the metrics used to determine cutoff values (wells flagged "cytotoxic/misdispensed").
Table S2. Statistics for the "Number of Detected Rosettes per Cell" metric used to determine active compound criteria.
Table S3. EC_{50} measurements for validated compounds.

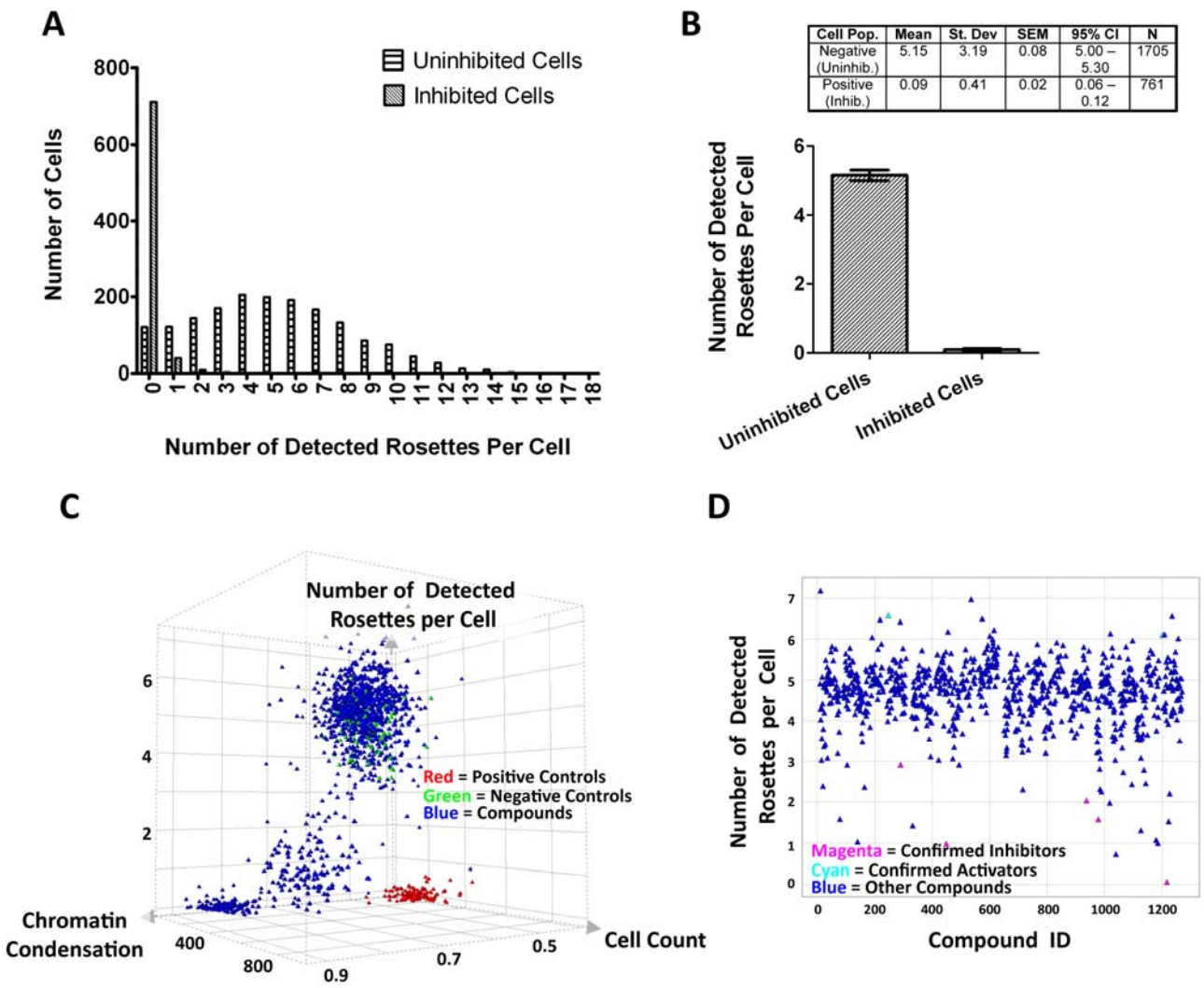

Cell Pop.	Mean	St. Dev	SEM	95% CI	N
Negative (Uninhib.)	5.15	3.19	0.08	5.00 – 5.30	1705
Positive (Inhib.)	0.09	0.41	0.02	0.06 – 0.12	761

Figure S1. Statistics of positive (inhibited) and negative (uninhibited) control cell populations for rosette detection.

Control cell populations utilized for this analysis were obtained by pooling cell-by-cell data from 3 randomly selected representative control wells for each population.

A. Distribution of the parameter "Number of Detected Rosettes per Cell" for control cell populations. The histogram shows "Frequency" (or count) on the y-axis versus the range of values encountered for the "Number of Detected Rosettes per Cell" parameter on the x-axis.

B. The panel displays the large difference of the "Number of Detected Rosettes per Cell"

parameter between the inhibited and uninhibited cell populations. Average and 95% confidence interval are shown in the bar graph. Also provided are the population statistics in the inset table. Note: This analysis refers to the cell-by-cell distribution of the rosette detection within well populations as opposed to the screen result distribution of well averages.

C. Scatter plots detailing the primary screen results. All data points represent the average value of the duplicate wells. The panel shows a 3D scatter plot of 3 of the metrics used to determine the primary screen active compound list (values provided in table S1). Several clusters of compounds can be visually distinguished: (i) mis-dispensed or toxic compounds were identified by low cell counts and high chromatin condensation; (ii) compounds with cytotoxic effects show average to low cell count or increased chromatin condensation in combination with smaller nuclei area (or both) (table S1); (iii) positive (inhibition) controls show a lower cell count in addition to inhibiting rosette formation because the control compound inhibits cell division; (iv) inactive compounds and negative controls.

D. The panel displays a 2D scatter plot of the primary assay read-out ("Number of Detected Rosettes per Cell") for each compound with the 5 confirmed inhibitors highlighted in magenta and the two confirmed activators highlighted in cyan. Compounds flagged as mis-dispensed or cytotoxic were excluded from this plot.

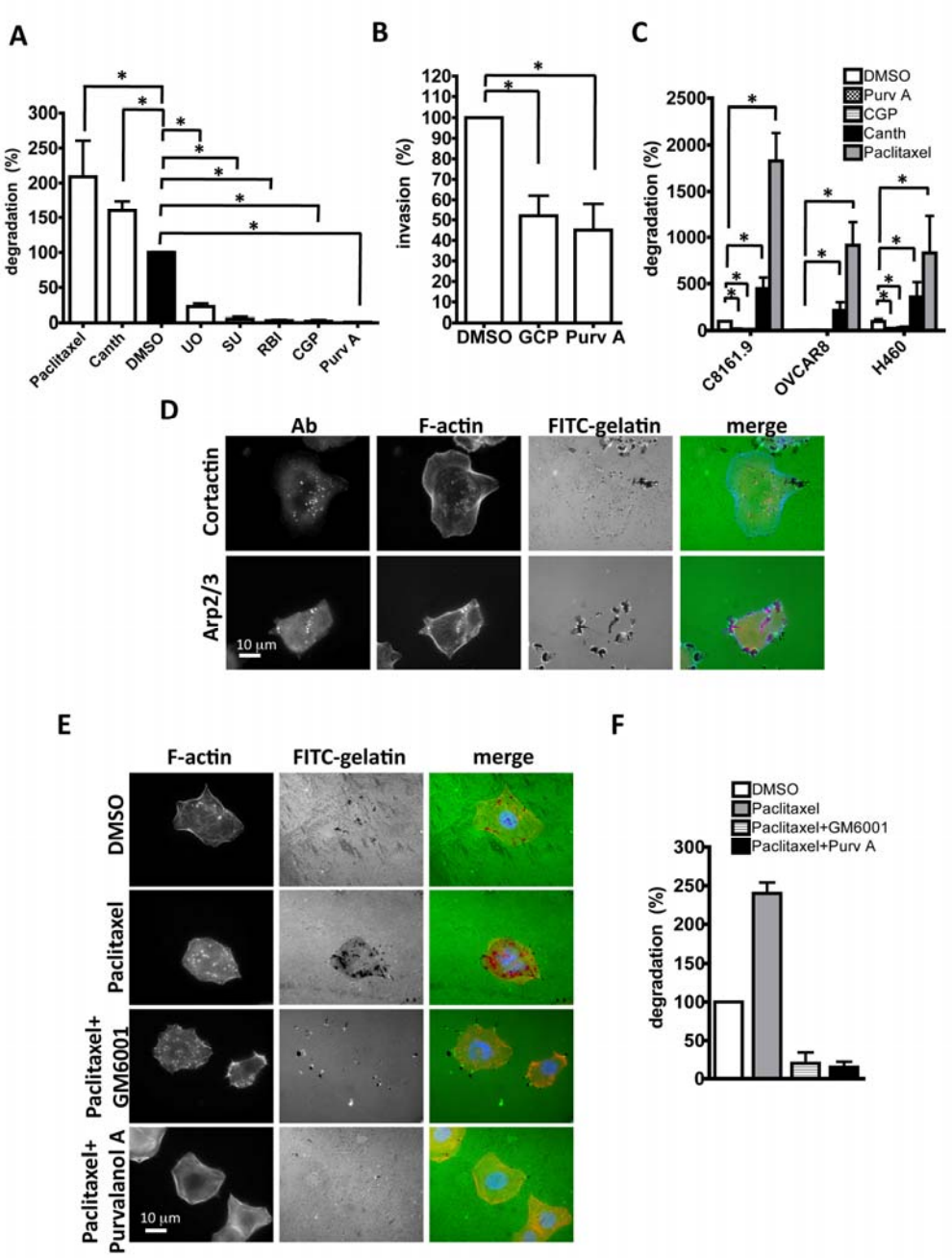

Figure S2. Detailed analysis of the HCS results.

A. Quantification of gelatin degradation (percent degraded area normalized to cell number) of Src-3T3 treated with active compounds at 10 μM. Compounds: paclitaxel, cantharidin (Canth), UO126 (UO), SU6656 (SU), 7-Cyclopentyl-5-(4-phenoxy)phenyl-7H-pyrrolo[2,3-d]pyrimidin-4-ylamine (RBI), GCP74514A (CGP), purvalanol A (PurvA).

B. Src-3T3 cells were treated with 5 μM of CGP and PurvA and assayed for matrigel invasion.

C. Quantification of gelatin degradation (percent degraded area normalized to cell number) of human cancer cell lines treated with active compounds at 2 μM.

D. Treatment of the paclitaxel-resistant ovarian cancer cell line TR-SKOV3 with 2 μM paclitaxel. Presence of invadopodia was determined by colocalization of F-actin and cortactin (upper row) or Arp2/3 (lower row) together with FITC-gelatin degradation.

E. Treatment of the SCC61 with different compounds. Presence of invadopodia was determined by F-actin staining together with FITC-gelatin degradation.

F. Quantification of gelatin degradation (percent degraded area normalized to cell number) of the experiment shown in the panel E.

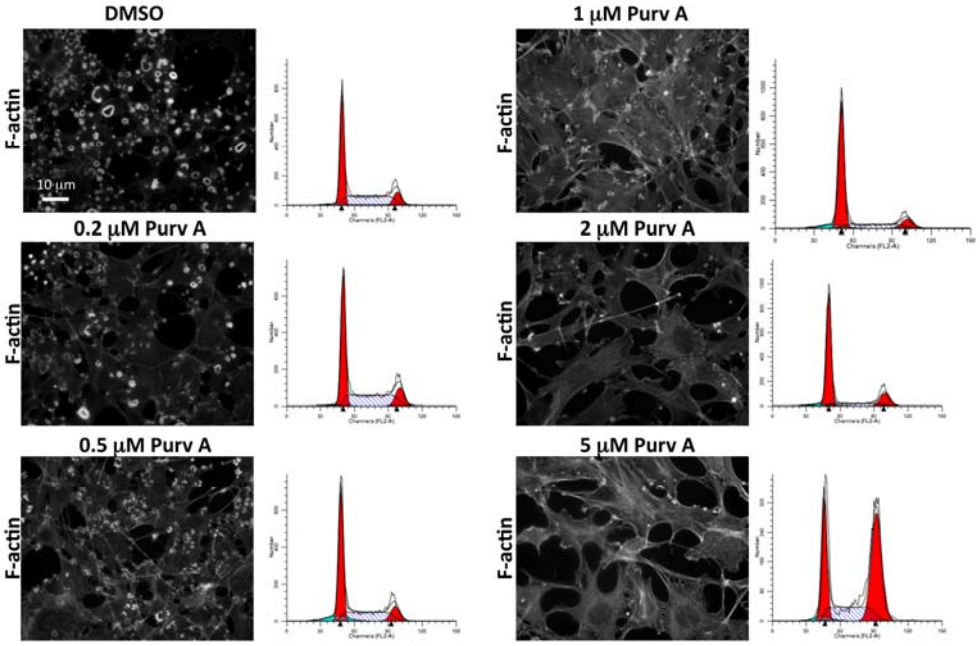

Figure S3. Effect of purvalanol A on the cell cycle.

Cells were treated with several concentrations of purvalanol A (Purv A) then assayed for invadopodia formation by phalloidin staining (F-actin) and cell cycle distribution by FACS analysis. The image analyses for different concentrations of purvalanol A (0, 0.2μM, 0.5μM, 1 μM, 2 μM, and 5 μM) are shown as insets.

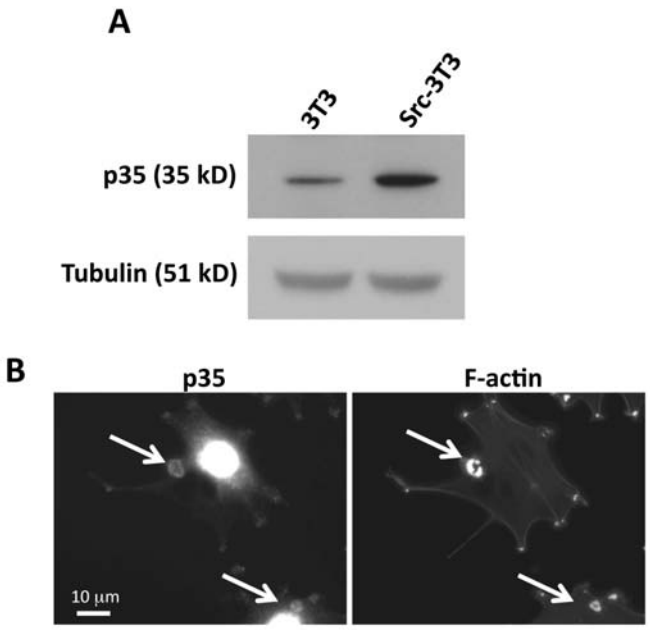

Figure S4. p35 abundance and localization in Src-3T3 cells.

A. Abundance of p35 protein in Src-3T3 cells compared with the parental 3T3 cell line.

B. Subcellular localization of p35. Src-3T3 cells were fixed and stained with phalloidin or with an antibody specific for p35 and processed for epifluorescence microscopy. Arrows indicate rosettes showing colocalization of F-actin and Cdk5.

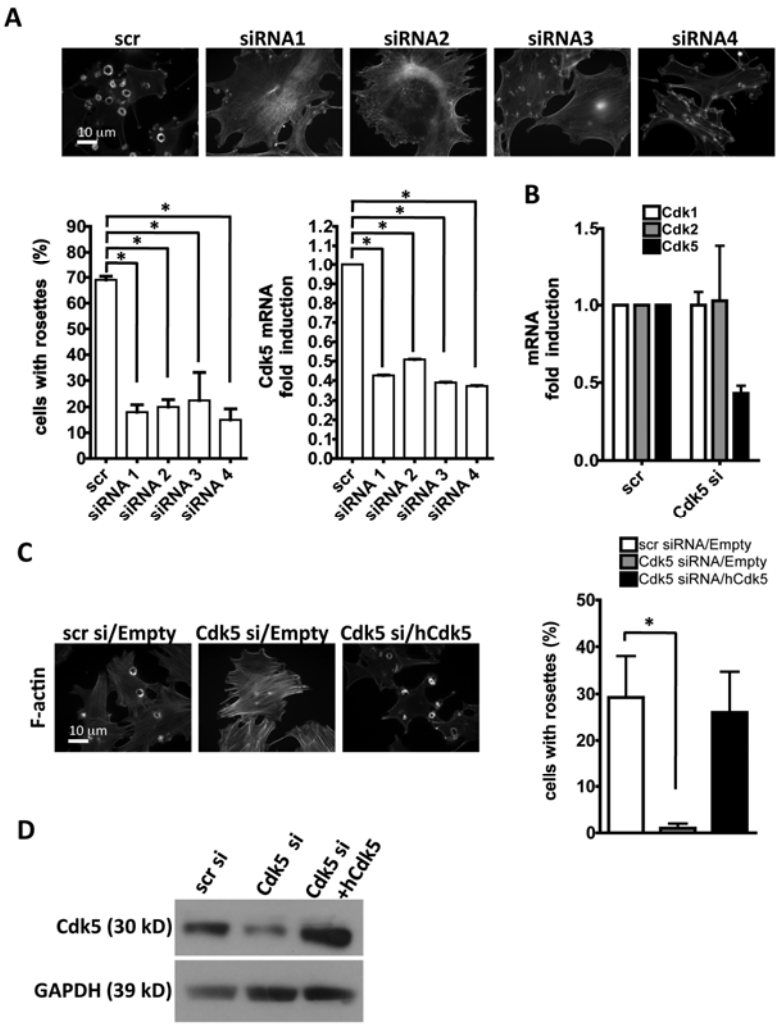

Figure S5. Effect of Cdk5 knockdown on formation and function of invadopodia.

A. Cells were transfected with scrambled or Cdk5-specific siRNAs (4 individual sequences) and assayed for formation of invadopodia by phalloidin staining (F-actin) (upper panels). Lower panels show the quantification of percentage of cells with invadopodia and Cdk5 knockdown.

B. mRNA abundance of Cdk1 and Cdk2 was determined in Cdk5 siRNA transfected cells.

C. Cells were transfected with recombinant human Cdk5 to re-introduce the protein after RNA interference, and assayed for formation of invadopodia by phalloidin staining (F-actin) (left panels). Right panel: quantification of percentage of cells with invadopodia.

D. Immunoblot showing Cdk5 abundance in the experiment described in panel C.

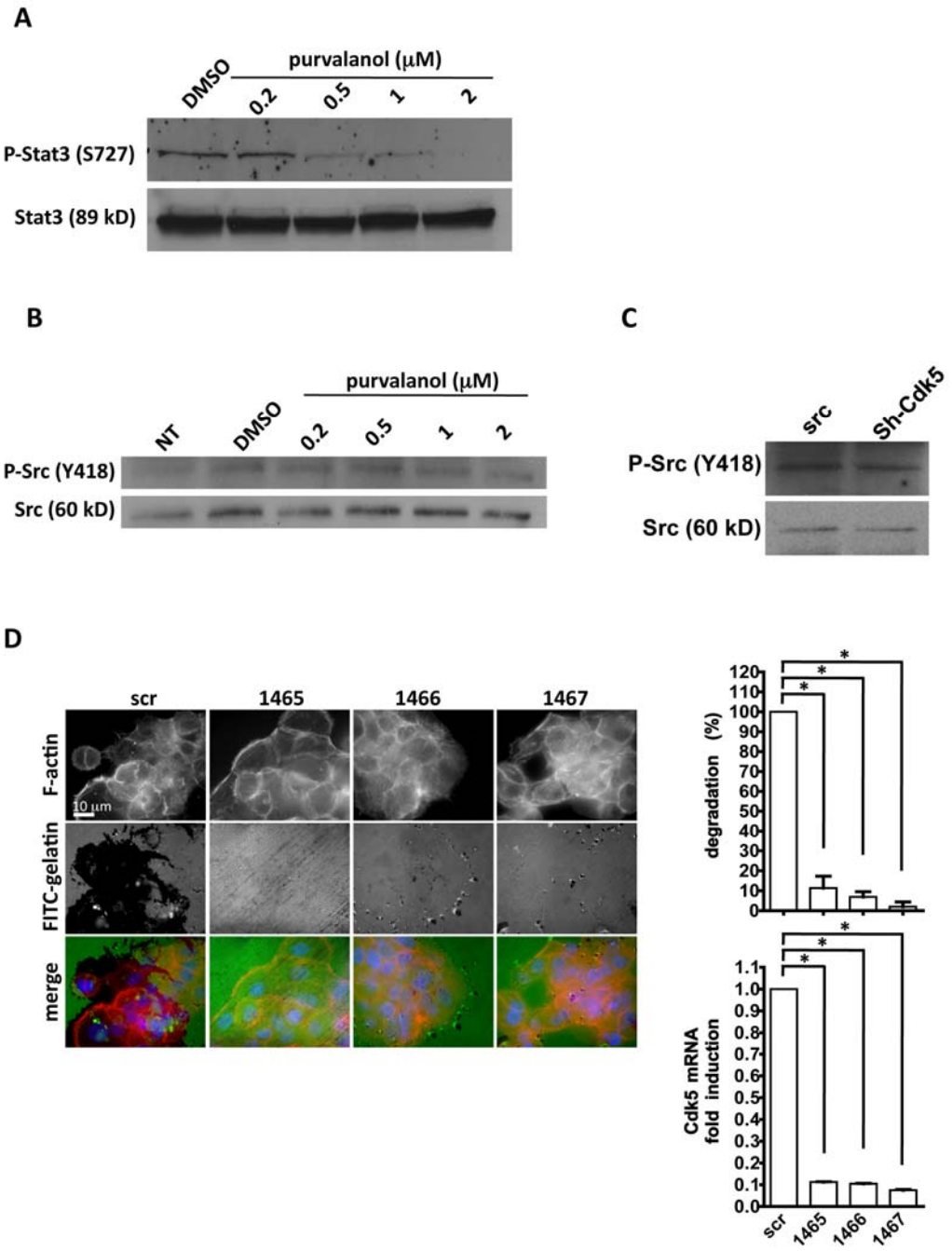

Figure S6. Effect of purvalanol A on Cdk5 activity.

A. The activity of Cdk5 was measured by determining the phosphorylation status of Stat3 at Ser^{727}, following treatment with several concentrations of purvalanol A.

B. The activity of Src was measured by determining the phosphorylation status of Tyr^{418}, following treatment with several concentrations of purvalanol A.

C. The activity of Src was measured by determining the phosphorylation status of Tyr^{418}, following siRNA knockdown of Cdk5.

D. SCC25 cells were infected with lentiviruses expressing scrambled control or three different Cdk5 shRNAs (1465, 1466, or 1467) and assayed for gelatin degradation (FITC-gelatin) (left panel). Right panels show quantification of gelatin degradation and knockdown of Cdk5 mRNA.

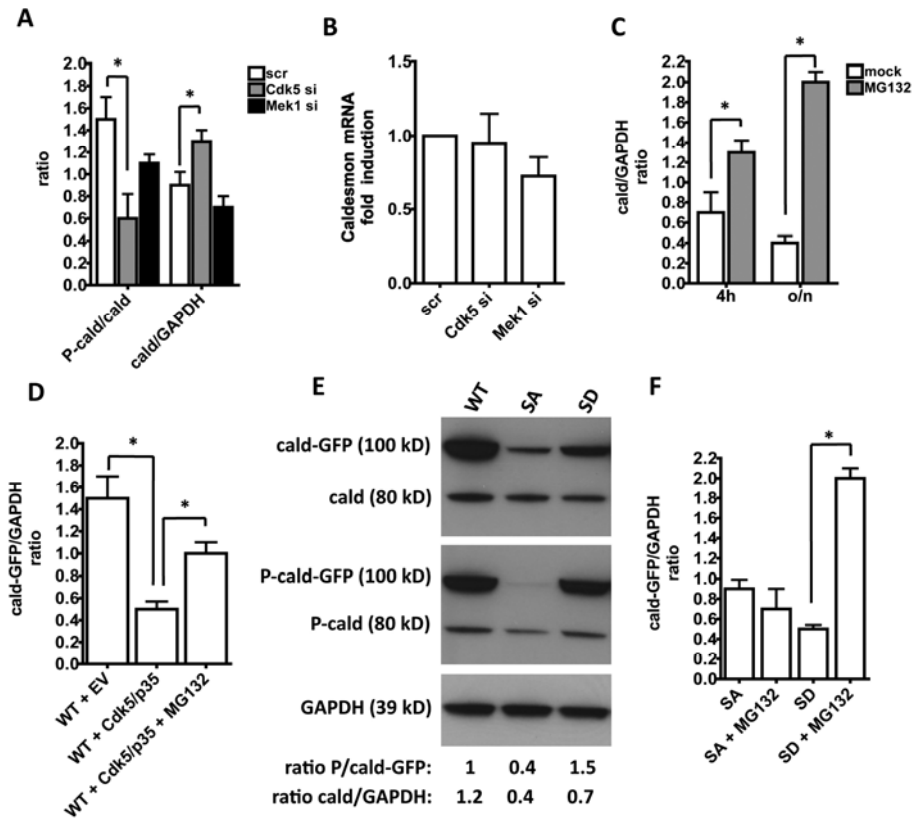

Figure S7. Phosphorylation of caldesmon by Cdk5 regulates formation of invadopodia.

A. Quantification of Fig. 5A, presented as mean ± SEM of three independent experiments.

B. Src-3T3 cells transfected with different siRNAs were subjected to RT-PCR analysis to determine the abundance of caldesmon mRNA.

C. Quantification of Fig. 5B, presented as mean ± SEM of three independent experiments.

D. Quantification of in Fig. 5C, presented as mean ± SEM of three independent experiments.

E. Immunoblot analysis of caldesmon phosphorylation in transfected Src-3T3 cells. Total cell extracts from cells transfected with various constructs were immunoblotted with antibodies that recognized phosphospecific (P-cald) and total (cald) caldesmon and GAPDH. The corresponding ratios of the digitized intensity of the GFP-tagged P-caldesmon variant to that of the GFP-tagged caldesmon are shown.

F. Quantification of Fig. 5D, presented as mean ± SEM of three independent experiments.

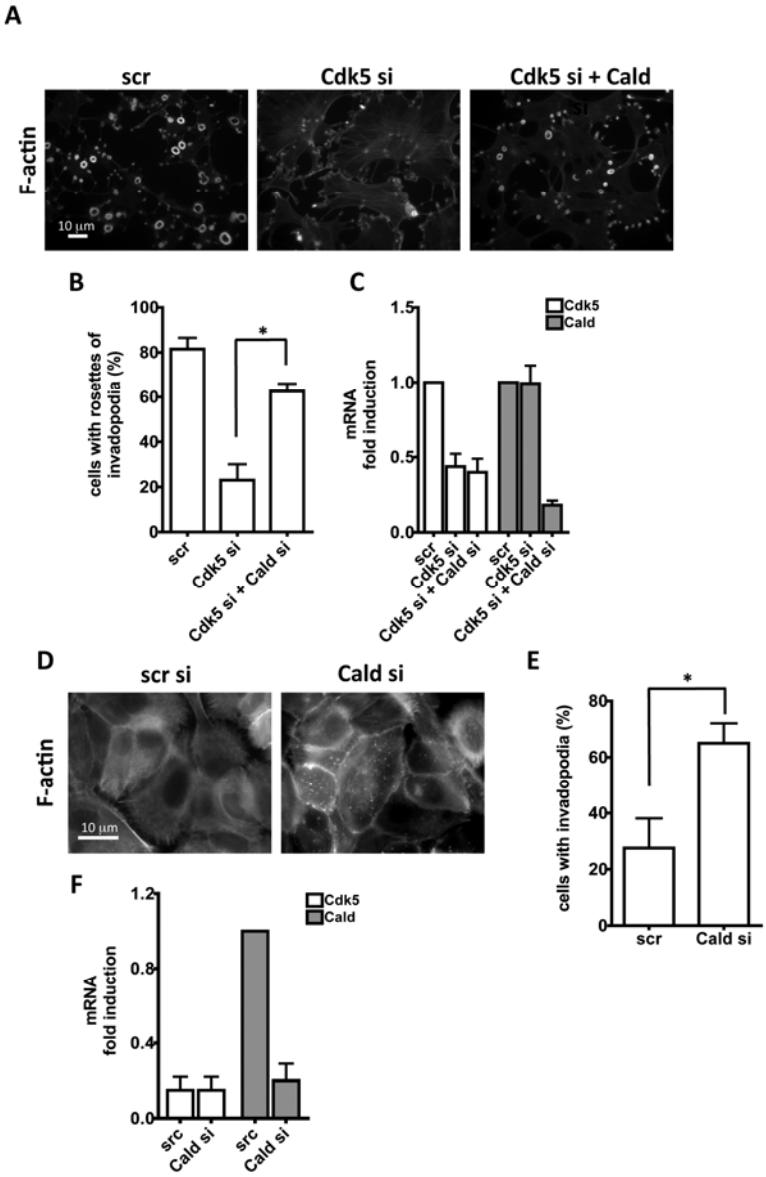

Figure S8. Knockdown of caldesmon rescues formation of invadopodia in cells deficient in Cdk5.

A. Src-3T3 cells were transfected with scrambled or Cdk5-specific siRNAs or a combination of Cdk5- and caldesmon-specific siRNAs and assayed for invadopodium formation by phalloidin staining (F-actin).

B. Quantification of percentage of cells with invadopodia.

C. Cdk5 and caldesmon mRNA abundance in cells in (A).

D. SCC61 cells stably expressing a Cdk5 specific shRNA (1465; Fig. 4) were transfected with

scrambled or caldesmon specific siRNAs and assayed for invadopodium formation by phalloidin staining (F-actin).

E. Quantification of percentage of cells with invadopodia in the different conditions noted.

F. Cdk5 and caldesmon mRNA abundance in cells in (D).

Table S1. Statistics for the metrics used to determine cutoff values (wells flagged "cytotoxic/misdispensed").

Metric:	Negative controls (mean)	Negative controls (SD)	Cut-off criteria	Calculated value	Selected cut-off
Cell count	567	104	<Mean – 3* SDs	255	250
Nuclear area	138.7	10.3	<Mean	138.7	135
&					&
Chromatin condensation	0.696	0.031	>Mean + 3* SDs	0.789	0.78

Table S2. Statistics for the "Number of Detected Rosettes per Cell" metric used to determine active compound criteria.

	Positive controls (mean)	Positive controls (SD)	Negative controls (mean)	Negative controls (SD)	Z' Value	<35% Inhibition	>35% Activation
Average of screen plates	0.238	0.159	4.433	0.606	0.446	2.97	5.87
Selected criteria	-	-	-	-	-	3	6

Table S3. EC_{50} measurements for validated compounds.

	EC_{50} (inhibition or activation of rosette formation)
Purvalanol A	0.2 μM
GCP74514A	0.2 μM
Cantharidin	2 μM
Paclitaxel	2 μM